Microchimica Acta (2020) 187:466
https://doi.org/10.1007/s00604-020-04433-1

ORIGINAL PAPER

Fluoroimmunoassay of influenza virus using sulfur-doped graphitic carbon nitride quantum dots coupled with Ag_2S nanocrystals

Ojodomo J. Achadu[1] · De Xing Lioe[2] · Keiichiro Kagawa[2] · Shoji Kawahito[2] · Enoch Y. Park[1,3]

Received: 18 April 2020 / Accepted: 7 July 2020

Abstract

Novel sulfur-doped graphitic carbon nitride quantum dots (S-gCNQDs) are synthesized using a single-source precursor in a one-step solvothermal process. The S-gCNQDs with a size of ~ 5-nm displayed a strong green intrinsic fluorescence at 512 nm when excited at 400 nm, with a quantum yield of ~ 33% in aqueous solution. The prepared S-gCNQDs and Ag_2S nanocrystals were applied as innovative functional materials to fabricate a biosensor for virus detection based on the conjugation of specific anti-human influenza A monoclonal antibody to the S-gCNQDs and Ag_2S NCs, respectively. In the presence of the influenza A virus, an interaction between the S-gCNQDs/Ag_2S-labeled antibody resulted in the formation of a nanosandwich structure, which is accompanied by the fluorescence enhancement of the S-gCNQDs. The change in fluorescence intensity linearly correlats with the concentration of the influenza A virus (H1N1) in the 10 fg/mL to 1.0 ng/mL range, with a limit of detection of 5.5 fg/mL. The assay was applied to the assay of clinically isolated influenza A virus (H3N2/Yokohama) mixed with human serum. The obtained limit of detection was 100 PFU/mL within the detection range of 10^2– 5×10^4 PFU/mL for the H3N2 virus.

Keywords Sulfur-doped graphitic carbon nitride QDs · Silver disulfide nanocrystals · Influenza A virus · Fluoroimmunoassay · Virus immunoassay · Localized surface plasmonic resonance · Nanosandwich complex

Introduction

Influenza virus emerged as a major epidemic over a decade ago and has remained a growing challenge to public health that needs responsive and accurate diagnostic measures to prevent the spread of the virus and promote early treatment [1]. Therefore, the current gold standard methods used for influenza virus immunoassays are enzyme-linked immunosorbent assay (ELISA), real-time reverse transcription-polymerase chain reaction (RT-qPCR), immunoblotting assays, and electrochemical sequence-specific genetic detection [2, 3]. Although these methods offer specific advantages and are widely used, nevertheless, they suffer some drawbacks due to high operating costs and, in some cases, high interference by complex matrices. It is, therefore, still necessary to implement cost-efficient methods.

The exceptional optoelectrical properties of fluorescent graphic carbon nitride quantum dots (gCNQDs) have earned

Electronic supplementary material The online version of this article (https://doi.org/10.1007/s00604-020-04433-1) contains supplementary material, which is available to authorized users.

✉ Enoch Y. Park
park.enoch@shizuoka.ac.jp

Ojodomo J. Achadu
ojodomo.john.achadu@shizuoka.ac.jp

De Xing Lioe
lioe@idl.rie.shizuoka.ac.jp

Keiichiro Kagawa
kagawa@idl.rie.shizuoka.ac.jp

Shoji Kawahito
kawahito@idl.rie.shizuoka.ac.jp

[1] Research Institute of Green Science and Technology, Shizuoka University, 836 Ohya, Suruga-ku, Shizuoka 422-8529, Japan

[2] Research Institute of Electronics, Shizuoka University, 3-5-1 Johoku, Nakaku, Hamamatsu, Shizuoka 432-8011, Japan

[3] Laboratory of Biotechnology, Department of Bioscience, Graduate School of Science and Technology, Shizuoka University, 836 Ohya, Suruga-ku, Shizuoka 422-8529, Japan

widespread interest in the design of promising fluorescent probes [4–6]. The synthesis of these carbon-based nanosized particles encompasses the "top-down and "bottom-up" approaches. The latter approach, which is ubiquitously deployed, involves the advanced chemical treatments by condensation and/or controlled pyrolysis of small and organically rich molecules such as formamide, urea, diaminomaleonitrile, melamine, guanidine, dicyandiamide, and organic amines [7–13]. Doping and/or heteroatom functionalization of carbon-based graphitic QDs has helped to improve their optical and electronic properties for various applications. For instance, sulfur-doped graphitic carbon nitride (gC_3N_4) nanosheets were prepared by the ball milling of melamine and sulfur powder for 48 h and subsequently treated under hydrothermal condition. The obtained nanosheets were deployed for enhanced electrocatalytic activity in fuel cells [14]. Phenyl-modified gC_3N_4, which showed a stoke shift of ~ 185 nm and a high fluorescence (FL) intensity, was prepared and used as a probe for thiram, a pesticide [15]. In another study, an electrochemical sensor for ascorbic acid (AA), dopamine, and uric acid was fabricated based on gC_3N_4 modified with graphene oxide [16]. A complex hybrid containing Cu-Pd nanoparticles was deposited on gC_3N_4 hybrid nanosheets for the colorimetric detection of glucose, taking advantage of the peroxidase mimic activity of the graphitic nanostructured composites [17]. In our previous studies, the facile one-step preparation of gCNQDs functionalized with thymine (T-gCNQDs) and tannic acid (TA-gCNQDs), respectively, was reported [9, 10]. The strongly fluorescent gCNQDs derivatives were deployed as highly competitive probes for Hg^{2+} and AA. However, innovative materials are still increasingly needed for the production of sensors/biosensors with real-time and realistic diagnostic applications. This ambition motivates the interest in the adoption of simple one-step in situ approaches for preparation of novel hybrid heteroatom-doped materials.

In this work, the analytical application of novel S-gCNQDs was examined by the fluoroimmunoassay of the influenza A virus as a test analyte. A fluoroimmunosensing method was developed by utilizing the metal-induced fluorescence enhancement of S-gCNQDs in the presence of Ag_2S nanocrystals (NCs). To develop the practical biosensor for influenza virus, novel S-gCNQDs and Ag_2S NCs, as innovative materials, were covalently conjugated, respectively, to specific anti-human influenza A monoclonal antibodies for the capture of the target influenza A virus. An immunoreaction ensued between the antibody-labeled S-gCNQDs/Ag_2S NCs in the presence of the influenza A virus. As a result, an immunocomplex structure was formed, followed by an enhancement of the fluorescence of the S-gCNQDs influenced by the proximity of Ag_2S NCs. The developed immunoassay is rapid and achieved a sensitive femtogram limit of detection (LOD) of 5.5 fg/mL for influenza A virus (H1N1). Also, clinically isolated influenza A virus (H3N2) was quantified down to 100 PFU/mL and shows that the developed system is highly sensitive compared with some commercially available rapid diagnostic test kits (with LODs of ~ 5000 PFU/mL). This system can be adapted for the versatile detection of other viral antigens by labeling the S-gCNQDs and Ag_2S NCs with suitable capture antibodies, which can induce the needed immuno-reactions.

Experimental

Chemicals and biological reagents/materials

Silver nitrate ($AgNO_3$), 3-mercaptopropionic acid (MPA, 99%), dimethyl formamide (DMF), bovine serum albumin (BSA), rhodamine 6G, N-hydroxysuccinimide (NHS), and N-(3-dimethylaminopropyl)-N′-ethylcarbodiimide hydrochloride (EDC) were purchased from Sigma-Aldrich (St Louis, USA, https://www.sigmaaldrich.com/). 4-Amino-3-hydrazino-5-mercapto-1,2,4-triazole; bovine serum albumin (BSA); 4-mercaptobenzoic acid (4-MBA); and NaOH were supplied by FUJIFILM Wako Pure Chemical Corporation (Osaka, Japan, http://ffwk.fujifilm.co.jp/en/index.html). Diethylene glycol (DEG) was purchased from Tokyo Chemical Industry (TCI) (Tokyo, Japan, https://www.tcichemicals.com/en/jp/).

Anti-human influenza A (H1N1) monoclonal antibody (clone C179), anti-human influenza A (H3N2) monoclonal antibody (Clone F49), and anti-human influenza A (H1, H2, H3) monoclonal antibody (Clone C111) which is positive for both influenza viruses H1N1 and H3N2 were purchased from Takara Bio. Inc. (Kusatsu, Shiga, Japan, https://www.takara-bio.com/). Influenza virus A/New Caledonia (20/99/IVR/116) (H1N1) was purchased from ProSpec-Tany TechnoGene Ltd. (Rehovot, Israel, https://www.prospecbio.com/). Human serum from human male AB plasma, USA origin, sterile-filtered was obtained from Sigma-Aldrich (St Louis, USA, https://www.sigmaaldrich.com/); dengue virus DNA was supplied by Integrated DNA Technologies (Iowa, USA) (www.idtdna.com). Clinically isolated influenza virus A/Yokohama/110/2009 (H3N2) was kindly provided by Dr. C. Kawakami of Yokohama City Institute of Health, Japan. Goat anti-rabbit IgG-HRP was purchased from Santa Cruz Biotechnology (Dallas, Texas, USA, https://www.scbt.com/home). Commercial RIDT kit - *QuikNavi Flu 2* was purchased from Denka -Seiken Co. Ltd. (Tokyo, Japan, http://denka-seiken.jp/jp/). For selectivity studies, Prof. K. Morita of Institute of Tropical Medicine, Nagasaki University, kindly provided the Zika virus used in this study. Noro virus-like particles (NoV-LPs) were prepared in our lab, according to the previously reported protocol [18]. Hepatitis E virus-like particles (HEV-LPs) were prepared according to the previous

report [19]. All experiments were carried out using high purity deionized (DI) water (> 18 MΩ cm). All detection/sampling protocol was carried out according to the standard protocol for influenza virus immunoassays [20].

Instrumentation

Ground-state electronic absorption (UV/vis), fluorescence excitation, and emission spectra were recorded on a filter-based multimode microplate reader (Infinite F200 M; TECAN, Ltd., Männedorf, Switzerland, https://www.tecan.com/). Images of the transmission electron microscope (TEM) were acquired using JEM-2100F operating at 100 kV (JEOL, Ltd., Tokyo, Japan, https://www.jeol.co.jp/en/products/detail/JEM-2100.html). Powder X-ray diffraction (PXRD) analysis was carried out using a RINT ULTIMA XRD (Rigaku Co., Tokyo, Japan, https://www1.rigaku.com/ja) with αNi filter and a Cu-Kα source. Data were collected over 2θ = 15–60° at a scan rate of 0.01°/step and 10 s/point. Dynamic light scattering (DLS) analysis was done on a Malvern Zetasizer nanoseries, Nano-ZS90 (Malvern Inst. Ltd., Malvern, UK, https://www.malvernpanalytical.com/). Fourier-transform infrared spectroscopy was performed using FT/IR-6300 with ATR PRO610P-S (JASCO, Tokyo, Japan, https://www.jasco.co.jp/). Raman spectroscopic measurements and surface-enhanced Raman scattering (SERS) experiment of 4-MBA (Raman reporter) and the virus-immunocomplex using Ag_2S NCs as the SERS substrate were carried out using NRS-7100 Raman Spectrometer with f500 spectrograph (JASCO, Tokyo, Japan). The measurements were done using a × 20 objective lens at 1% laser power and 2-s integration time. Fluorescence lifetime imaging microscopy (FLIM) experiment for lifetime determination was done using a Nikon Eclipse Ti-U microscope with a Nikon CFI S Plan Fluor ELWD 40x (NA = 0.60) and Hamamatsu C8898 (wavelength, 374 nm; pulse width, 74 ps; peak power, 47 mW) as the laser source (Hamamatsu, Japan). The FLIM camera used was a lab-made camera with a custom CMOS image sensor. The images were acquired by the FLIM CMOS camera via the Framelink PCIe card (VCE-CLEX02). The FLIM CMOS camera has a pixel array of 128 × 128 pixels; each has a four-tap pixel with a pitch of 22.4 μm × 22.4 μm. The sensor response time is 170 ps, measured with a 472-nm laser diode. Details of the phasor plots generation are given in Electronic Supporting Information (ESM). Conjugation of the antibody to the individual nanoparticles was confirmed by enzyme-linked immunosorbent assay (ELISA) using a microplate (Model 680; Bio-Rad, Hercules, USA, https://www.bio-rad.com/en-us/).

Synthesis of S-gCNQDs

Sulfur-doped graphitic carbon nitride QDs (S-gCNQDs) were prepared by the solvothermal treatment of a novel precursor, i.e., a mercapto-based triazole compound (Scheme 1). Briefly, 4-amino-3-hydrazino-5-mercapto-1,2,4-triazole (50 mg) and citric acid (5 mg) were dissolved in 10 mL of DMF, and the mixture was sonicated for 20 min to obtain a suspension. The resulting mixture was transferred and sealed in a 50-mL Teflon-lined stainless steel autoclave and heated at 200 °C for 8 h. The autoclave was allowed to cool naturally, and the obtained product was filtered through a 0.22-μm microporous filter membrane and then dialyzed for 2 days using a dialysis tubing membrane-MWCO 2.0 kDa to obtain pure S-gCNQDs solution. The solution was further freeze-dried to obtain a solid product.

Ag_2S NCs were synthesized according to procedures reported previously with some modification [21]. Detailed synthesis procedures are presented in Electronic Supporting Information (ESM).

Antibody conjugation process and virus detection

First, anti-human influenza virus A (H1N1) (clone C179) or (H1, H2, H3) (clone C111) monoclonal antibody was conjugated onto the surface of S-gCNQDs or Ag_2S NCs via EDC/NHS chemistry. To achieve this, 100 μL of 0.1 M EDC was added to 2 mL (0.1 mg/mL) of S-gCNQDs to activate the carboxylic groups on their surface, and the solution was stirred for 1 h, followed by the addition of 100 μL of 0.1 M NHS to the mixture and the stirring continued for another 1 h. Then, 5.1 μg/mL of the antibody (prepared in PBS 7.6) was added to the activated S-gCNQDs, and the resulting mixture was stirred for 8 h at 7 °C. Anti-human influenza virus A (H3N2) monoclonal antibody (clone F49) was also conjugated to S-gCNQDs for the detection of the clinically isolated influenza virus A/Yokohama/110/2009 (H3N2). Similar procedures were followed for the antibody conjugation of the Ag_2S NCs but using anti-human influenza virus A (H1, H2, H3) (clone C111) monoclonal antibody instead of anti-human influenza virus A (H1N1) (clone C179). The obtained antibody-conjugated S-gCNQDs or Ag_2S NCs were purified by centrifugation (3000×*g*, 5 min) to remove unbound antibodies followed by incubation with 5% BSA (for blocking) to ensure non-specific binding interactions. Excess BSA was further removed by centrifugation, and the conjugates redissolved in ultra-pure DI water for further use.

Following the antibody conjugation, the virus assay was carried out using different concentrations of influenza A virus (H1N1) within the range from 1.0 fg/mL to 10 ng/mL. Typically, in a 96-well plate, 100 μL of the antibody-conjugated S-gCNQDs (2.0 mg/mL in PBS, pH 7.6) was incubated with 100 μL of each concentration (1, 10, 10^2, 10^3, 10^4, 10^5, 10^6 fg/mL) of the influenza A/New Caledonia virus

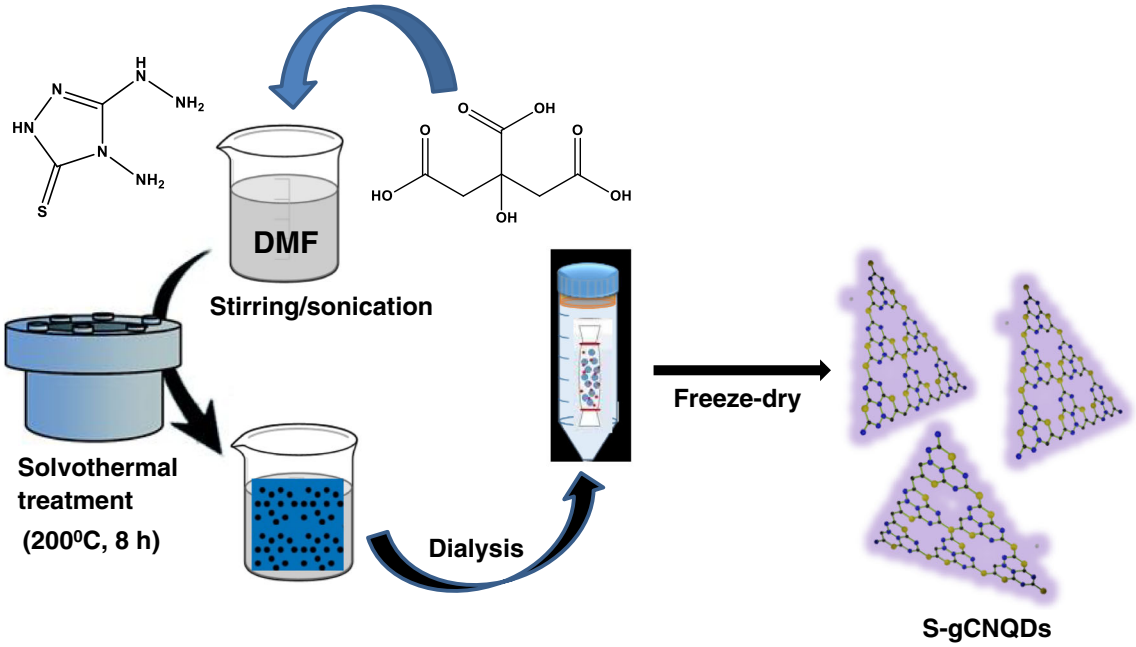

Scheme 1 Synthesis pathway of S-gCNQDs

(H1N1) for 2 min. Then, 50 μL of the antibody-conjugated-Ag_2S (1 mg/mL in PBS, pH 7.6) was added to the mixture and shaken for 5 min to induce the virus-mediated nanosandwich complex formation. Then, the FL intensity change of the S-gCNQDs in the hybrid sandwich nanostructure was measured at the 400-nm excitation wavelength, with maximum emission intensity at 512 nm to construct a calibration curve.

The analysis of clinically isolated influenza A/Yokohama (H3N2) was assayed using similar procedures upon mixing with human serum. One hundred microliters of the antibody-conjugated S-gCNQDs (2.0 mg/mL in PBS, pH 7.6) was mixed with 50 μL of the clinical samples dissolved in PBS (pH 7.6) in 40% diluted human serum and incubated for 2 min. This solution was followed by the addition of 50 μL of the antibody-conjugated-Ag_2S NCs (1 mg/mL in PBS, pH 7.6) and then thoroughly shaken for 5 min and allowed for about further 10 min before the FL signals were collected at 512-nm emission wavelength upon excitation at 400 nm. The detected range was within 20–50,000 PFU/mL of the clinical samples. All detection experiments were done in triplicate under a similar procedure and at optimized conditions (See ESM for details).

Results and discussion

Choice of materials

The surface functionalization and/or doping of carbon-based QDs with heteroatoms (S, N, and B) are known to result in substantial improvements in their optical properties and performance [22–24]. This is because their optical properties are altered by the introduction of "emissive trap sites" and/or "surface defects," which influence the radiative recombination of their excitons [25, 26]. This work presents an exceptionally rich novel source precursor for the preparation of gCNQDs with heteroatoms (S and N) functionality using 4-amino-3-hydrazino-5-mercapto-1,2,4-triazole. This compound contains a high percentage of the amino group (NH_2) (essential for covalent attachments) and N-atoms linked in a triazole ring with extended C–N and C=S linkages (Scheme 1). The S, N-derived gCNQDs herein have a significant advantage which is the connective affinity to interact with Au or Ag-based nanoparticles to form functional hybrids. In addition to the presence of a planar graphitic structure for non-covalent π stacking interactions, S-gCNQDs prepared using this precursor possesses more than one point of attachment for simple surface modifications and hybrid nanostructuring choices.

On the other hand, plasmonic semiconductor nanostructures can act as nanoantennas when close to fluorophores resulting in changes in their optical properties. This mostly leads to a favorable effect known as metal-enhanced fluorescence (MEF) [27–29]. This type of influence has been used in detection systems where metallic nanostructures regulate the emissions of colloidal quantum dots [28]. Semiconductor nanocrystals such as Ag_2S NCs used in this work are known to exhibit tunable plasmonic properties in the near-infrared (NIR) region and are excellent nanostructures for various optical-based signal enhancement processes such as MEF, SERS, and photocatalysis [28–32]. It is in this light that we deployed Ag_2S NCs in this work to push the fluorescence detection sensitivity of S-gCNQDs for the detection of influenza virus via metal-based enhancement of their fluorescence by controlling the local environment surrounding the S-gCNQDs via immuno-reactions with influenza virus, as a test analyte.

Synthesis and characterization of novel S-gCNQDs and Ag_2S nanocrystals

The precursor for the S-doped gCNQDs was 4-amino-3-hydrazino-5-mercapto-1,2,4-triazole. This precursor was inspired by its high nitrogen/sulfur content and relatively low cost. Hence, the solvothermal treatment and condensation of the heterocyclic triazole ring of the precursor to achieving novel S-gCNQDs follow a similar formation mechanism as outlined in literature for the synthesis of gCNQDs using other triazole compounds [7, 8, 12, 13].

To characterize the prepared S-gCNQDs, TEM was employed, and the image acquired shows a quasi-spherical morphology of the S-gCNQDs. They appear to be monodispersed with sizes typically estimated within the range of 3–5 nm (Fig. 1a). To supplement the information on the size determination from the TEM micrograph, the DLS experiment revealed that the average size distribution of the gCNQDs was ~ 5.5 nm (Fig. 1b). This result is in close agreement with the size distribution obtained using TEM images and further indicates sizes typical of carbon-based QDs [7, 9, 10]. XRD pattern obtained for the S-gCNQDs displayed a broad diffraction peak at $2\theta = 27°$, which is indexed as (002) lattice typical of graphitic carbon nitrides (g-C_3N_4) (Fig. 2a) [7, 12, 13]. This diffraction peak corresponds well in intensity and position with the known *d*-spacing and disordered nanostructure of g-C_3N_4, thus indicating their formation. Fourier-transform infrared (FTIR) spectroscopy further revealed the base structure of the S-doped gCNQDs derivative. As shown in Fig. 2b, the observed vibration at 662 cm^{-1} is assigned to the formed heptazine units of the S-gCNQDs. Characteristic absorption bands of C=N/C–C and C–N stretching modes of the graphitic structure were observed at 1493, 1387, and 1097 cm^{-1}, respectively. At 1628 cm^{-1}, asymmetric vibrations referring to the carboxylic groups introduced by citric acid as co-precursor are conspicuously observed. Intense broad peak typical of the –N–H (resulting from the 2° or 3° amine moieties) and/or hydroxyl (OH) of the carboxylic group vibrations have been observed around 3715–2985 cm^{-1} as well as characteristic –CH_2 peaks of the triazine rings at 2930 and 2897 cm^{-1}. The presence of the S-atom was confirmed by the appearance of a strong C=S absorption at 1248 cm^{-1}, with an accompanying weak vibration of the C–S bond at 859 cm^{-1} (Fig. 2b). The Raman spectra (Fig. 2c) of the solvothermally prepared S-gCNQDs displayed the characteristic bands indexed at ~ 1345 (D band) and ~ 1586 cm^{-1} (G band) due to the disordered sp^2 as a result of the C–N linkage and graphitic sp^2 layer nanostructures, respectively [7–10, 12, 13]. These results confidently show that S-gCNQDs were successfully prepared using the novel precursor.

The ground-state absorption recorded for the prepared S-gCNQDs is reminiscent of the electronic transition (π–π^*) of the s-triazine units of the carbon nitride family [33–35]. An intense absorption occurred in the region < 500 nm. Therefore, the S-gCNQDs were subjected to different excitation wavelengths (350 to 500 nm) to determine the optimum emission intensity and wavelength. At an excitation wavelength of 400 nm, the emission intensity was maximum and occurred at ~ 512 nm. Next, the evaluation of the relative fluorescence quantum yield (Φ_F) of the material was calculated to be ~ 33% using rhodamine 6G as the reference standard (see Electronic Supporting Information for details). The value of Φ_F for the prepared S-gCNQDs (using 4-amino-3-hydrazino-5-mercapto-1,2,4-triazole as the source of S and N) is higher than that reported using other source precursors such as urea (17.9%), melamine (5.5%), or formamide (29%) [7, 36, 37]. It is demonstrated in this work that the use of 4-amino-3-hydrazino-5-mercapto-1,2,4-triazole results in a graphitic QDs with FL emission extending into the green region of the visible spectrum which are desired for various applications.

Furthermore, fluorescence lifetime imaging microscopy (FLIM) experiments were conducted to determine the lifetime of the prepared S-gCNQDs. This measurement was carried out using the frequency-domain FL lifetime determination

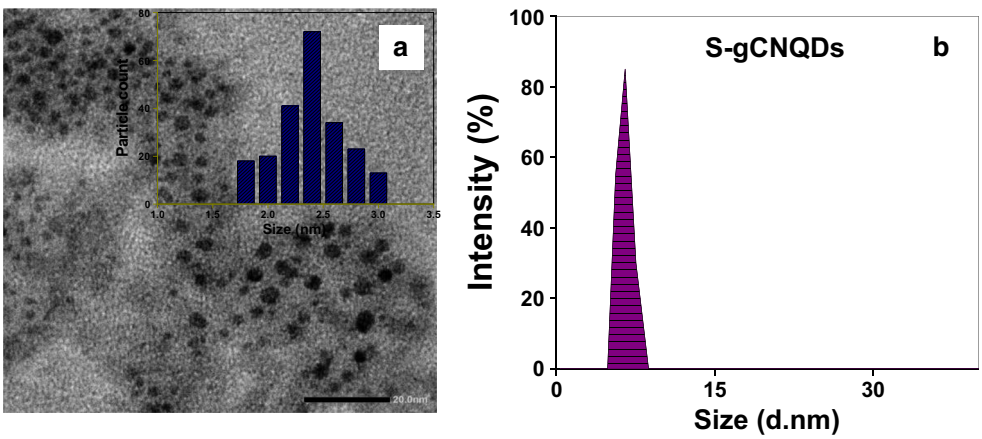

Fig. 1 **a** TEM image of S-gCNQDs (inset is the size distribution histogram). **b** DLS graph of S-gCNQDs

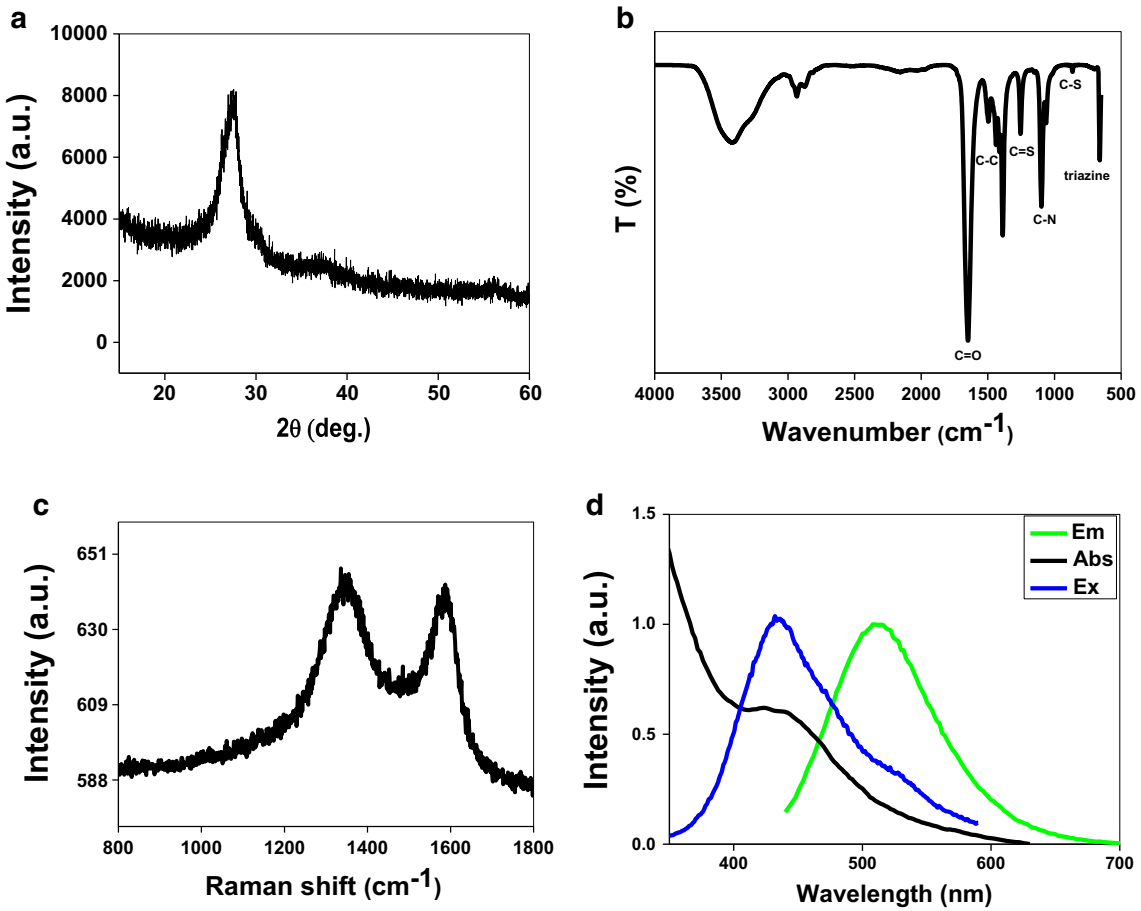

Fig. 2 Characterization spectra of S-gCNQDs showing **a** XRD pattern. **b** FTIR absorptions. **c** Raman spectra and **d** UV-Vis, excitation, and emission spectra (solvent:DI water). $\lambda_{ex} = 400$ nm

known as the phasor approach [38, 39]. This approach, which differs from time-correlated single-photon counting method, is accomplished by analyzing the FLIM data in phasor space by observing the clustering of pixel values (from images) in some areas of the generated phasor plots rather than by fitting the fluorescence decay using exponentials. As shown in Fig. 3a, the second (*) and third (#) peaks from the measured waveform are due to crosstalk between different taps in the pixel of the acquired images. This is then deconvoluted to obtain the result, Fig. 3b. The average value of the two-component decay lifetime of S-gCNQDs was determined to be 3.19 ns. The FLIM measurement results of S-gCNQDs and their immunocomplexes in the presence of the target virus are shown in Fig. S3 in Electronic Supporting Information (ESM).

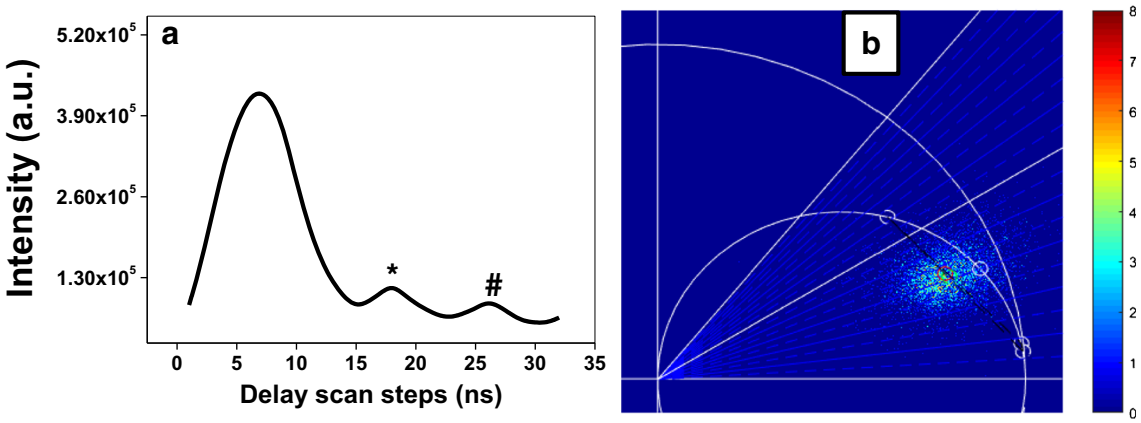

Fig. 3 **a** FL lifetime decay of pristine S-gCNQDs. **b** Phasor plot showing the decay component for the analyzing frequency of 20 MHz

Detailed Ag_2S NCs characterization data, experimental results demonstrating their plasmonic/optical properties, and discussion are presented in Electronic Supporting Information (ESM).

Sensitive fluoroimmunoassay

Influenza A/New Caledonia virus (H1N1) was detected based on preliminary studies using Ab-conjugated S-gCNQDs in the presence of Ab-Ag_2S NCs to form a nanosandwich complex leading to signal-amplified fluorescence cycles which are dependent on the concentrations of the target influenza virus A(H1N1) (Fig. 4a). The influenza A virus (H1N1) detection was initially carried out in DI water, and the recorded FL intensities are shown in Fig. 4a. Also, since the human serum is a mixture of complex biological compounds as matrices, the influenza A/New Caledonian (H1N1) virus was assayed in human serum (40%) to simulate the conditions close to actual clinical samples. Hence, it was observed that the S-gCNQDs could respond to the presence of the influenza A virus (H1N1) within the linear concentration range of 10 fg/mL to 1 ng/mL (Fig. 4b). The detection sensitivity of the probe towards the target virus (H1N1) was evaluated by the construction of a calibration plot using Eq. (1) [40].

$$\frac{\Delta F}{F_0} = 0.1 + K\,[\text{virus}] \quad (1)$$

where ΔF is the difference between FL intensity before (F_0) and after (F) addition of virus, K is the fluorescence enhancement factor. [Virus] is the concentration of the target virus. The expression $\Delta F/F_0 = (F_{\text{with virus}} - F_0)/F_0$ gives a ratio of the fluorescence enhancement to the fluorescence signal before virus addition (F_0) [41].

Overall, the increased concentrations of influenza A virus (H1N1) led to a proportional enhancement in the FL intensity of S-gCNQD measured in DI water and human serum, respectively. Interestingly, the sensitivity achieved in both media showed an only but slight difference, with similar linearity of their calibration plots (Fig. 4b). The analytical figures of merit of the assay were assessed by calculating the limits of detection (LODs) using the equation (LOD = 3δ/K) [42], where the standard deviation (δ) of 10 replicated measurements (n = 10) was taken. K is the value of the slopes of the linear calibration plots. The LOD was calculated to be 5.5 fg/ml in DI water and 8.5 fg/ml in human serum, respectively (Table S1).

Detailed results and discussion of optimization and control studies leading to the established detection of influenza virus in work are given in the Electronic Supporting Information (ESM).

Assay of clinically isolated influenza virus (H3N2)

To detect clinically isolated influenza A virus (H3N2), the S-gCNQDs modified with the H3N2 monoclonal antibody was employed (instead of H1N1 monoclonal antibody) in the presence of the Ab-Ag_2S NCs to form a sandwich nanocomplex. It was observed that the Ab (H3N2)-conjugated S-gCNQDs responded to the presence of the influenza A virus (H3N2) within the linear concentration range of 100–50,000 PFU/mL (Fig. 5a). The detection sensitivity of the probe towards clinically isolated influenza A virus (H3N2) was evaluated by the construction of a calibration plot (Fig. 5a inset), using Eq. (1) above. The calculated LOD was 100 PFU/mL. Also, human serum was spiked with a known concentration of the clinically isolated influenza A (H3N2). The assay was able to quantify ~ 98% of the virus with good recoveries (Table S2). Therefore, the performance of the developed detection platform for the influenza virus was further evaluated against a commercial rapid influenza diagnostic kit (RIDT) – *QuikNavi-Flu* 2 (Denka Seiken Co. Ltd., Tokyo, Japan). The clinical samples assayed using the RIDT showed that influenza virus A/Yokohama/110/2009 (H3N2) samples with ≥ 1000 PFU/mL could only be detected. As shown in Fig. S4, influenza virus A/Yokohama/110/2009 (H3N2) is not detectable at < 1000 PFU/mL by the RIDT kit. Meanwhile, our developed biosensor for the influenza virus is responsive to the H3N2 viral RNA down to 45 PFU/mL. This result indicates that our detection system can achieve an upwards of ~ 10 times more sensitivity when used in place of the commercial RIDT. It should be pointed out, however, that both detection strategies are, in theory, very different, and the production of a fast

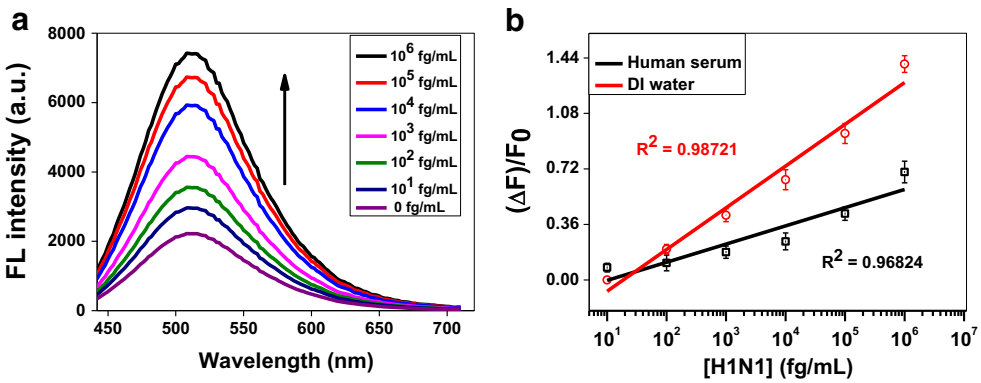

Fig. 4 **a** Detection FL spectra of S-gCNQDs showing enhancement in intensity at various H1N1 virus concentrations. **b** The corresponding calibration plots generated in DI water and human serum. λ_{ex} = 400 nm

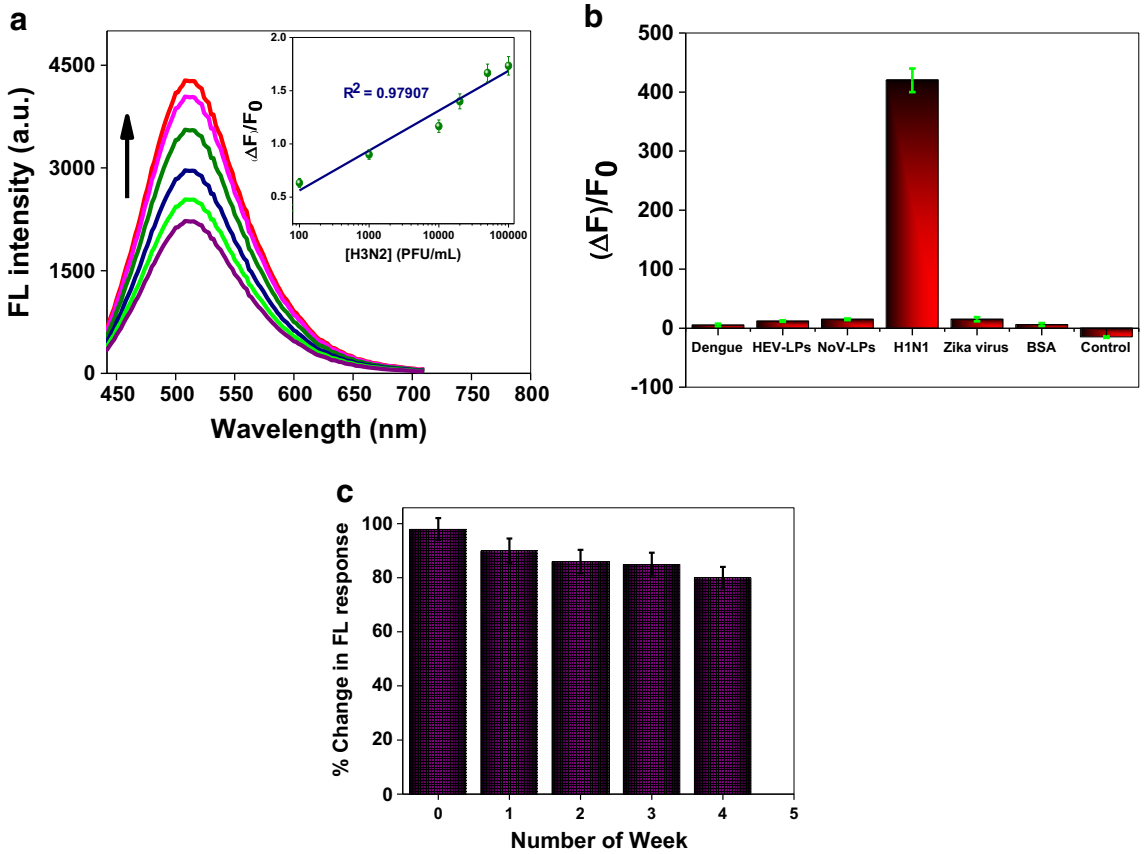

Fig. 5 **a** FL spectra for the detection of clinically isolated influenza A virus (H3N2). Inset: the corresponding calibration plot. **b** Plots showing H1N1 selective assay in the presence of other viruses/V-LPS. **c** Stability test of S-gCNQDs and Ag_2S NCs with 1 ng/mL of H3N2 virus showing percentage change in FL signal response over 4 weeks. $\lambda_{ex} = 400$ nm

diagnostic kit with our designed system will enhance the sensitive detection of the influenza virus considerably. Furthermore, clinical samples containing target influenza virus can be assayed rapidly in ~ 15 min, which is quite preferable to the clinical used RT-PCR or rapid molecular assays capable of producing results in approximately 15–30 min and other molecular assays capable of detecting RNA or nucleic acid influenza in around 45–80 min [2, 3].

Selectivity

The selectivity of the developed assay was probed in the presence of NoV-LPs, Zika virus, HEV-LPs, and dengue DNA to establish the extent of the selective nature of the test. Expectedly, no interferences and/or changes occurred in the fluorescence signal of S-gCNQDs even to 1 ng/mL of the tested virus and V-LPs (Fig. 5b). This observation can be attributed to the specific affinity of the influenza A virus to bind to the antibody functionalized nanoparticles (S-gCNQDs/Ag_2S NCs). This affinity is as a result of the induced changes in the FL intensity of the S-gCNQDs signals compared with when other non-specific viruses interact with S-gCNQDs. It is pertinent to state here that this system may present a versatile detection approach for desired viruses by choosing the appropriate antigen-antibody pair for the sandwich immuno-reactions leading to the sensitive detection of the mediating virus.

However, the proposed assay herein has some limitations. The sensitivity of this assay is majorly limited by the interference of heavy metals such as Hg^{2+} and Cd^{2+} ions, which can quench the FL of the S-gCNQDs. Also, the sizes of the S-gCNQDs and Ag_2S NCs may need to be carefully controlled to achieve the sandwich formation in the presence of the target virus. Clinical samples matrix interference may impair the sensitivity of detection. To address this, a magnetic separation protocol/virus enrichment should be considered.

Detection mechanism

In view of the observed FL enhancement in S-gCNQDs when immunocomplex with influenza virus in the presence of Ag_2S NCs, it was speculated that aggregation-induced emission and/or metal-plasmonic enhancement effects might be responsible for the FL signal enhancement. However, results obtained from the TEM image of the immunocomplex (Fig. S5 in Electronic Supporting Information) showed no clear evidence

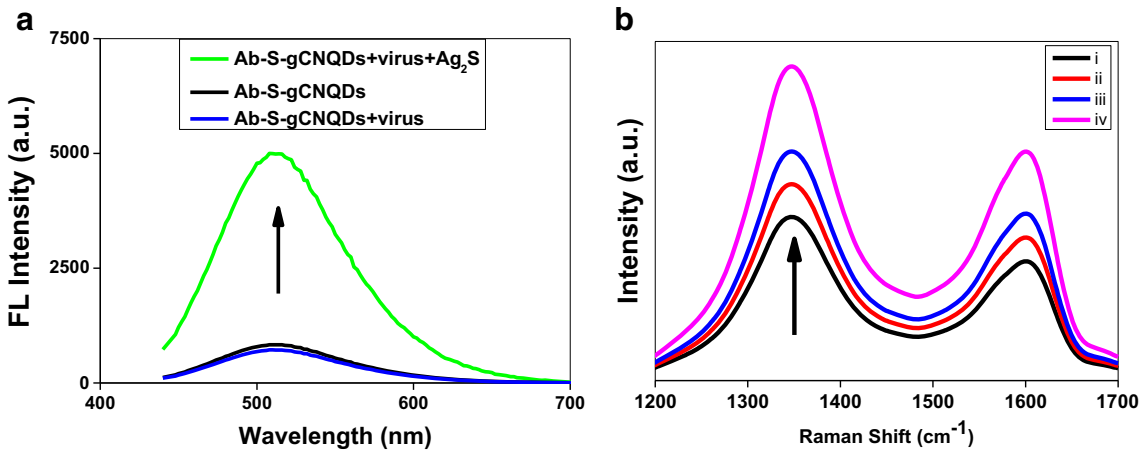

Fig. 6 **a** Fluorescence signal enhancement of S-gCNQDs in the presence of Ag_2S NCs. **b** Corresponding SERS enhancement of S-gCNQDs at different concentrations of Ag_2S NCs due to local optical coupling effects

of aggregation of nanoparticles of S-gCNQDs or Ag_2S NCs in the presence of the target virus. This outcome diverted our attention to the possibility of an optical-based enhancement mechanism since the plasmonic properties of Ag_2S NCs have been reported previously [43, 44]. Raman measurement and SERS analysis were carried out (detailed results and discussion are presented in Electronic Supporting Information). To elucidate the detection mechanism of the developed immunoassay by evaluating the plasmonic and/or optoelectronic coupling effects of Ag_2S NCs, the SERS experiments were carried out further complement the observed FL enhancement of S-gCNQDs (Fig. 6), the detailed SERS results and discussion of 4-MBA are shown in Fig. S6 of Electronic Supporting Information. The results plausibly demonstrated that the coupling interactions between S-gCNQDs and Ag_2S NCs via plasmonic and/or chemical interaction resulted in the observed SERS signal enhancement of S-gCNQDs, similar to report for GQDs in the presence of plasmonic nanostructures [45]. Therefore, it is credible to state that the enhanced SERS signals from the S-gCNQDs/Ag_2S NCs virus-mediated immunocomplex are due to the local optical field created by electronic interaction between the S-

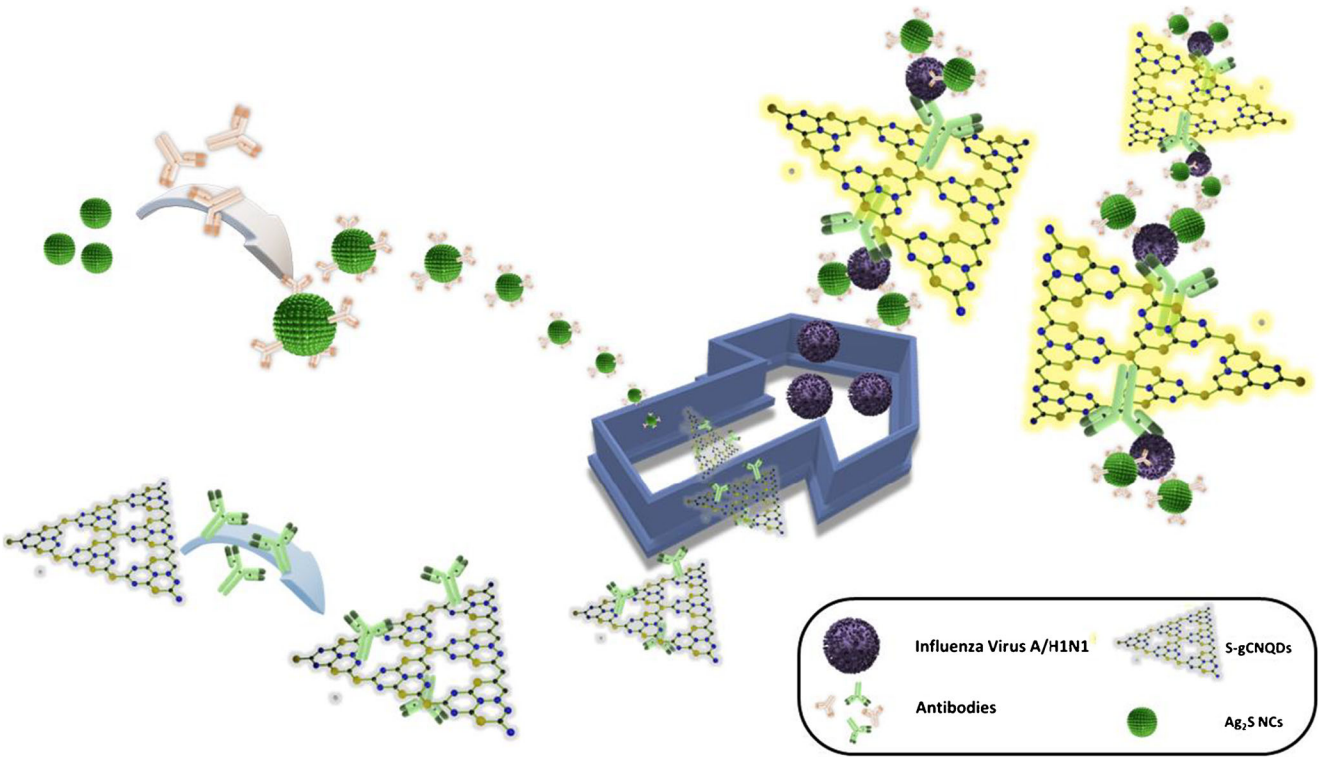

Scheme 2 Schematic representation of the S-gCNQDs and Ag_2S modification with antibody and the detection protocol by sandwich nanostructure formation in the presence of target influenza A virus

gCNQDs and Ag_2S NCs. This process might be responsible for the enhancement of the fluorescence signals of the S-gCNQDs resulting from their proximity to Ag_2S NCs in a sandwiched network triggered by the target virus (Scheme 2). Overall, these findings and the control experiments lead us to conclude that Ag_2S NCs influenced the enhancement of the fluorescence of S-gCNQDs regulated by the target influenza virus, which resulted in the sensitive detection of the virus.

Conclusion

In this work, a functional and innovative combination of S-doped graphitic QDs and Ag_2S nanocrystals are deployed for the fluoroimmunoassay of the influenza A virus. The S-doped graphitic QDs which were prepared using a novel precursor via a rapid one-step solvothermal route, displayed excellent optical properties. Their functionalization with specific antibodies positive for the target virus initiated a virus-regulated interaction between the S-doped graphitic QDs and Ag_2S nanocrystals. This resulted in the fluorescence enhancement of S-gCNQDs upon forming an immunocomplex with the influenza virus in the presence of Ag_2S nanocrystals. The fluorescence of S-gCNQDs increased consistently as the concentration of the virus increased, thus leading to the rapid detection of the target influenza virus in a highly sensitive and selective manner. The materials herein present an opportunity to fabricate a novel biosensing platform required for practical detection of the influenza virus and for testing other potentially harmful infectious diseases. This assay is rapid, convenient, and versatile as specific proteins and virus-like particles of clinical interests can conceivably be expanded when the materials are functionalized with capture antibody of interest.

Acknowledgments The authors sincerely thank Professor K. Morita of the Institute of Tropical Medicine, Nagasaki University, for providing the Zika virus. Dr. C. Kawakami of Yokohama City Institute of Health, Japan, is gratefully acknowledged for providing the clinically isolated influenza virus A/Yokohama/110/2009 (H3N2). We also wish to thank Dr. T.C. Li of the National Institute for Infectious Disease of Japan for providing HEV-LPs.

Funding information O.J.A and S. K. gratefully acknowledge the Japan Society for the Promotion of Science (JSPS) for a Postdoctoral Fellowship for Research in Japan (Standard) (Grant No. 19F19348) and the Grant-in-Aid for Scientific Research (S) (Grant No. 18H05240), respectively.

Compliance with ethical standards

Competing interests The authors declare that they have no conflict of interest.

Ethical approval This study was approved and carried out according to the guidelines provided by the Ethics Committee of the Environment and Hygiene Institute in Shizuoka Prefecture (September 14, 2016).

Conflict of interest The authors declare that they have no competing of interests.

References

1. Gatherer G (2009) The 2009 H1N1 influenza outbreak in its historical context. J Clin Virol 45:174–178
2. Dziąbowska K, Czaczyk E, Nidzworski D (2018) Detection methods of human and animal influenza virus-current trends. Biosensors 8:94. https://doi.org/10.3390/bios8040094
3. Choi YJ, Kim HJ, Park JS, Oh MH, Nam HS, Kim YB (2010) Evaluation of new rapid antigen test for detection of pandemic influenza A/H1N1 2009 virus. J Clin Microbiol 48:2260–2262. https://doi.org/10.1128/JCM.02392-09
4. Dong Y, Wang Q, Wu H, Chen Y, Lu CH, Chi Y, Yang HH (2016) Graphitic carbon nitride materials: sensing, imaging and therapy. Small 12:5376–5393
5. Ahmad R, Tripathy N, Khosla A, Khan M, Mishra P, Ansari WA, Syed MA, Hahn YB (2020) Recent advances in nanostructured graphitic carbon nitride as a sensing material for heavy metal ions. J Electrochem Soc 167:037519
6. Cheng Q, He Y, Ge Y, Zhou J, Song G (2018) Ultrasensitive detection of heparin by exploiting the silver nanoparticle-enhanced fluorescence of graphitic carbon nitride (g-C_3N_4) quantum dots. Microchim Acta 185:332–340
7. Barman S, Sadhukhan M (2012) Facile bulk production of highly blue fluorescent graphitic carbon nitride quantum dots and their application as highly selective and sensitive sensors for the detection of mercuric and iodide ions in aqueous media. J Mater Chem 22:21832–21837
8. Tang Y, Su Y, Yang N, Zhang L, Lv Y (2014) Carbon nitride quantum dots: a novel chemiluminescence system for selective detection of free chlorine in water. Anal Chem 86:4528–4535
9. Achadu OJ, Revaprasadu N (2019) Tannic acid-derivatized graphitic carbon nitride quantum dots as an "on-off-on" fluorescent nanoprobe for ascorbic acid via copper(II) mediation. Microchim Acta 186:87–97. https://doi.org/10.1007/s00604-018-3203-x
10. Achadu OJ, Revaprasadu N (2018) Microwave-assisted synthesis of thymine-functionalized graphitic carbon nitride quantum dots as fluorescent nanoprobe for mercury(II). Microchim Acta 185:461–469
11. Xu J, Chen Y, Ma D, Shang JK, Li YX (2017) Simple preparation of MgO/g-C_3N_4 catalyst and its application for catalytic synthesis of dimethyl carbonate via trans-esterification. Catal Commun 95:72–76
12. Li Y, Cai J, Liu F, Yu H, Lin F, Yang H, Lin Y, Li S (2018) Highly crystalline graphitic carbon nitride quantum dots as a fluorescent nanosensor for detection of Fe(III) via an inner filter effect. Microchim Acta 185:134–140
13. Liu S, Tian J, Wang L, Luo Y, Sun X (2012) A general strategy for the production of photoluminescent carbon nitride dots from organic amines and their application as novel peroxidase-like catalysts for colorimetric detection of H_2O_2 and glucose. RSC Adv 2:411–413
14. Xu C, Han Q, Zhao Y, Wang L, Li Y, Qu L (2015) Sulfur-doped graphitic carbon nitride decorated with graphene quantum dots for an efficient metal-free electrocatalyst. J Mater Chem A 3:1841–1846

15. Mei H, Shu H, Lv H, Liu MW, Wang X (2020) Fluorescent assay based on phenyl-modified g-C_3N_4 nanosheets for determination of thiram. Microchim Acta 187:159–167
16. Zhang L, Liu C, Wang Q, Wang X, Wang S (2020) Electrochemical sensor based on an electrode modified with porous graphitic carbon nitride nanosheets (C_3N_4) embedded in graphene oxide for simultaneous determination of ascorbic acid, dopamine and uric acid. Microchim Acta 187:149–159. https://doi.org/10.1007/s00604-019-4081-6
17. Darabdhara G, Boruah PK, Das MR (2019) Colorimetric determination of glucose in solution and via the use of a paper strip by exploiting the peroxidase and oxidase mimicking activity of bimetallic Cu-Pd nanoparticles deposited on reduced graphene oxide, graphitic carbon nitride, or MoS_2 nanosheets. Microchim Acta 186:13–23. https://doi.org/10.1007/s00604-018-3112-z
18. Ahmed SR, Takemura K, Li TC, Kitamoto N, Tanaka T, Suzuki T, Park EY (2017) Size-controlled preparation of peroxidase-like graphene-gold nanoparticle hybrids for the visible detection of norovirus-like particles. Biosens Bioelectron 87:558–565
19. Li TC, Yamakawa Y, Suzuki K, Tatsumi M, Razak M, Uchida T, Takeda N, Miyamura T (1997) Expression and self-assembly of empty virus-like particles of hepatitis E virus. J Virol 71:7207–7213
20. World Health Organization (2017) WHO information for the molecular detection of influenza viruses July [accessed 5 June 2020] http://www.who.int/influenza/gisrs_laboratory/WHO_information_for_the_molecular_detection_of_influenza_viruses_20171023_Final.pdf
21. Jiang P, Zhu CN, Zhang ZL, Tian ZQ, Pang DW (2012) Water-soluble Ag_2S quantum dots for near-infrared fluorescence imaging in vivo. Biomaterials 33:5130–5135
22. Bankole OM, Achadu OJ, Nyokong T (2017) Nonlinear interactions of zinc phthalocyanine-graphene quantum dots nanocomposites: investigation of effects of surface functionalization with heteroatoms. J Fluoresc 27:755–766
23. Qu D, Zheng M, Du P, Zhou Y, Zhang L, Li D, Tan H, Zhao Z, Xied Z, Sun Z (2013) Highly luminescent S, N co-doped graphene quantum dots with broad visible absorption bands for visible light photocatalysts. Nanoscale 5:12272–12277
24. Holá K, Sudolská M, Kalytchuk S, Nachtigallová D, Rogach AL, Otyepka M, Zbořil R (2017) Graphitic nitrogen triggers red fluorescence in carbon dots. ACS Nano 12:12402–12410
25. Gu SY, Hsieh CT, Gandomi YA, Chang JK, Li J, Li JL, Zhang HA, Guo Q, Lau KC, Pandey R (2019) Microwave growth and tunable photoluminescence of nitrogen-doped graphene and carbon nitride quantum dot. J Mater Chem C 7:5468–5476
26. Wang J, Cao S, Ding Y, Ma F, Lu W, Sun M (2016) Theoretical investigations of optical origins of fluorescent graphene quantum dots. Sci Rep 6:24850–24855
27. Lakowicz JR, Ray K, Chowdhury M, Szmacinski H, Fu Y, Zhang J, Nowaczyk K (2008) Plasmon-controlled fluorescence: a new paradigm in fluorescence spectroscopy Analyst, 133: 1308–1346
28. Deng W, Xie F, Baltar HTMCM, Goldys EM (2013) Metal-enhanced fluorescence in the life sciences: here, now and beyond. Phys Chem Chem Phys 15:15695–15708
29. Faucheaux JA, Stanton ALD, Jain PK (2014) Plasmon resonances of semiconductor nanocrystals: physical principles and new opportunities. J Phys Chem Lett 5:976–985. https://doi.org/10.1021/jz500037k
30. Lee SH, Nishi H, Tatsuma T (2017) Tunable plasmon resonance of molybdenum oxide nanoparticles synthesized in non-aqueous media. Chem Commun 53:12680–12683
31. Zhang J, Pan Y, Chen Y, Lu H (2018) Plasmonic molybdenum trioxide quantum dots with noble metal-comparable surface enhanced Raman scattering. J Mater Chem C 6:2216–2220
32. Zhou Y, Li W, Zhang Q, Yan S, Cao Y, Dong F, Wang F (2017) Non-noble metal plasmonic photocatalysis in semimetal bismuth films for photocatalytic NO oxidation. Phys Chem Chem Phys 19:25610–25616. https://doi.org/10.1039/C7CP04359G
33. Achadu OJ, Nyokong T (2017) In situ one-pot synthesis of graphitic carbon nitride quantum dots and its 2, 2, 6, 6-tetramethyl (piperidin-1-yl) oxyl derivatives as fluorescent nanoprobes for ascorbic acid. Anal Chim Acta 991:113–126
34. Zhou J, Yang Y, Zhang CY (2013) A low-temperature solid-phase method to synthesize highly fluorescent carbon nitride dots with tunable emission. Chem Commun 49:8605–8607
35. Liu S, Wang L, Tian J, Zhai J, Luo Y, Lu W, Sun X (2011) Acid-driven microwave-assisted production of photoluminescent carbon nitride from N,N-dimethylformamide. RSC Adv 1:951–953
36. Guo J, Lin Y, Huang H, Zhang S, Huang T, Weng W (2017) One-pot fabrication of fluorescent carbon nitride nanoparticles with high crystallinity as a highly selective and sensitive sensor for free chlorine. Sensors Actuators B Chem 244:965–971
37. Rong M, Lin L, Song X, Wang Y, Zhong Y, Yan J, Feng Y, Zeng X, Chen X (2015) Fluorescence sensing of chromium (VI) and ascorbic acid using graphitic carbon nitride nanosheets as a fluorescent switch. Biosens Bioelectron 68:210–217
38. Digman MA, Caiolfa VR, Zamai M, Gratton E (2008) The phasor approach to fluorescence lifetime imaging analysis. Biophys J 94: 14–16
39. Chen H, Ma N, Kagawa K, Kawahito S, Digman M, Gratton E (2018) Wide-field multi-frequency fluorescence lifetime imaging using a two-tap complementary metal-oxide semiconductor camera with lateral electric field charge modulators. J Biophotonics 12:1–9
40. Lakowicz JR (2009) Principles of fluorescence spectroscopy, Third edn. Springer, New York, p 243
41. Lee J, Ahmed SR, Oh S, Kim J, Suzuki T, Parmar K, Park S, Lee J, Park EY (2015) A plasmon-assisted fluoro-immunoassay using gold nanoparticle-decorated carbon nanotubes for monitoring the influenza virus. Biosens Bioelectron 64:311–317
42. Lima KMG, Raimundo IM Jr, Pimentel MF (2007) Improving the detection limits of near infrared spectroscopy in the determination of aromatic hydrocarbons in water employing a silicone sensing phase, Sens. Actuators B Chem 125:229–233
43. Hou X, Zhang X, Yang W, Liu Y, Zhai X (2012) Synthesis of SERS active Ag_2S nanocrystals using oleylamine as solvent, reducing agent and stabilizer. Mater Res Bull 47:2579–2583
44. Fang C, Lee YH, Shao L, Jiang R, Wang J, Xu QH (2013) Correlating the plasmonic and structural evolutions during the sulfidation of silver nanocubes. ACS Nano 7:9354–9365. https://doi.org/10.1021/nn404042p
45. Zou F, Zhou H, Van Tan T, Kim J, Koh K, Lee J (2015) Dual-mode SERS-fluorescence immunoassay using graphene quantum dot labeling on one-dimensional aligned magnetoplasmonic nanoparticles. ACS Appl Mater Interfaces 7:12168–12175. https://doi.org/10.1021/acsami.5b02523